

See discussions, stats, and author profiles for this publication at: <https://www.researchgate.net/publication/335198132>

Hydrogenated C60 as high-capacity stable anode materials for Li-ion batteries

Article · August 2019

DOI: 10.1021/acsaem.9b01040

CITATIONS

2

READS

52

8 authors, including:



Joseph Teprovich

California State University, Northridge

40 PUBLICATIONS 613 CITATIONS

[SEE PROFILE](#)



Patrick A Ward

Savannah River National Laboratory

16 PUBLICATIONS 276 CITATIONS

[SEE PROFILE](#)



Chengxi Huang

Virginia Commonwealth University

29 PUBLICATIONS 330 CITATIONS

[SEE PROFILE](#)



Jian Zhou

Xi'an Jiaotong University

85 PUBLICATIONS 2,482 CITATIONS

[SEE PROFILE](#)

Some of the authors of this publication are also working on these related projects:



Direct LiT Electrolysis for Fusion Energy [View project](#)



Google [View project](#)

1 Hydrogenated C₆₀ as High-Capacity Stable Anode Materials for Li 2 Ion Batteries

3 Joseph A. Teprovich, Jr.,^{*,†} Jason A. Weeks,[‡] Patrick A. Ward,[§] Spencer C. Tinkey,[§]
4 Chengxi Huang,^{||,⊥} Jian Zhou,^{⊥,#} Ragaiy Zidan,[§] and Puru Jena^{*,⊥,#}

5 [†]Department of Chemistry and Biochemistry, California State University Northridge, Northridge, California 91330, United States

6 [‡]Department of Chemistry, The University of Texas at Austin, Austin, Texas 78712, United States

7 [§]Savannah River National Laboratory, Aiken, South Carolina 29803, United States

8 ^{||}Department of Applied Physics and Institution of Energy and Microstructure, Nanjing University of Science and Technology,
9 Nanjing, Jiangsu 210094, P. R. China

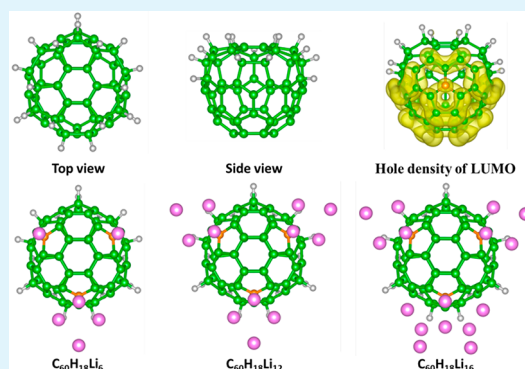
10 [⊥]Department of Physics, Virginia Commonwealth University, Richmond, Virginia 23284, United States

11 [#]Center for Advancing Materials Performance from the Nanoscale, State Key Laboratory for Mechanical Behavior of Materials, Xi'an
12 Jiaotong University, Xi'an 710049, P. R. China

13 **S** Supporting Information

14 **ABSTRACT:** There is a need to develop high-capacity and stable anode
15 materials for the next generation of lithium ion batteries that will power
16 consumer electronics and of automobiles of the future. This report
17 describes a systematic experimental and theoretical evaluation of a series
18 of hydrogenated fullerenes (C₆₀H_x) for use as high-capacity anodes in
19 lithium ion batteries. It was discovered that there is an optimal number of
20 hydrogen atoms that must be chemically bonded to C₆₀ to achieve
21 reversible lithiation. Under the optimized conditions, C₆₀H_x was found to
22 have a stable capacity of 588 mAh/g for over 600 cycles at a current
23 density of 0.05 A/g. Extended cycling studies at higher current densities
24 demonstrated that this material is stable for 2000 cycles. Theoretical
25 modeling of this system determined that electronic structure changes due
26 to hydrogenation is responsible for the favorable interaction of Li⁺ with
27 C₆₀H_x. This study represents a unique methodology for increasing anode
28 capacity and optimization of an anode's electrochemical properties by controlling the hydrogen content of the active material.

29 **KEYWORDS:** fullerene, anode, hydrogen, lithium ion battery, intercalation, electrochemistry



30 ■ INTRODUCTION

31 The increased power demands of advanced consumer
32 electronics has led to the search for materials that can enable
33 higher capacity, safer, and longer lasting lithium ion batteries
34 (LIB). In order for the next generation of LIB to achieve these
35 demands, there is a need to replace the graphite anode which
36 has a theoretical capacity of 372 mAh/g based on one lithium
37 ion stored per six carbon atoms (Li:6C) in the charged state.
38 Additionally, the lithiation potential of graphite is close to the
39 reduction potential of lithium, possibly leading to plating of
40 lithium on the electrode. This could produce lithium dendrites
41 that can puncture the polyethylene separator leading to a short
42 circuit and fire in the battery. This has also led to the extensive
43 investigation and commercialization of LIB with lithium
44 titanate (LTO) as an anode. The lithiation of LTO occurs at
45 much higher potentials than graphite (1.5 V vs Li⁺/Li), which
46 eliminates the possibility of lithium dendrite formation.
47 However, the LTO anode has a much lower capacity than
48 graphite (175 mAh/g vs 372 mAh/g), and a full cell would

operate at a much lower potential (~2.4 V vs ~3.7 V when
paired with a cathode such as LiCoO₂).

Early research on C₆₀ demonstrated that it is a suitable host
matrix for various alkali metals resulting in a superconducting
phase (M₃C₆₀) with a critical temperature (T_c) greater than
100 K under certain conditions.^{1–3} This ability of C₆₀ to act as
a robust host of alkali and alkaline earth ions promoted its
investigation as an anode for lithium, sodium, potassium, and
magnesium ion intercalation.^{4–11} However, pure C₆₀ is not
suitable as an anode material in commonly used liquid
electrolyte systems in metal ion batteries (i.e., LiPF₆ in
ethylene carbonate:dimethyl carbonate). After the intercalation
of the metal cation, the resulting M_xC₆₀ material becomes
soluble in the polar organic electrolyte solution, resulting in the
dissolution of the electrode with cycling. This has limited the

Received: May 28, 2019

Accepted: August 15, 2019

Published: August 15, 2019



64 use of pure C_{60} anodes with polymer-based electrolytes in
65 solid-state cells to overcome the solubility issue of the M_xC_{60}
66 with varying degrees of success.^{12–17} Functional groups have
67 also been attached to the C_{60} molecule (carboxyl, ester, and
68 piperazine) through multistep synthetic methods and utilized
69 as anodes.¹⁸ The ester-functionalized C_{60} showed the highest
70 reversible capacity (861 mAh/g specific capacity with 60 wt %
71 active material in the electrode) after 100 cycles with 0.1 C
72 cycling rate. This behavior is attributed to the ability of ester
73 groups (or carboxylate groups) to bind lithium ions, donate
74 electrons to the C_{60} cage, and increase the lattice void space
75 and specific surface area for lithium intercalation.

76 Recently the M_xC_{60} class of materials have attracted great
77 interest as hydrogen storage materials through the reversible
78 formation of a metal intercalated fullerane ($M_xC_{60}H_y$).^{19–21}
79 The presence of the intercalated alkali metal facilitates the
80 reversible formation of covalent C–H bonds on the C_{60} at
81 relatively low temperatures and pressures. In $M_xC_{60}H_y$, it has
82 been experimentally and theoretically shown that the
83 intercalated alkali metal dictates the sites at which the
84 formation of the C–H bond will occur on the C_{60} . Some
85 experimental results suggest that complete hydrogenation of
86 the C_{60} , formation of $C_{60}H_{60}$, is possible for the Na_6C_{60}
87 system.²² These studies clearly demonstrated a strong link
88 between the ability of C_{60} to reversibly chemisorb hydrogen
89 and the stoichiometric ratio of the alkali metal. Intrigued by
90 these findings, we investigated the opposite—how does the
91 presence of chemisorbed hydrogen on the surface of C_{60} affect
92 its ability to intercalate alkali metal ions as an anode material?

93 To date, there have only been two studies to evaluate the
94 electrochemical intercalation of hydrogenated fullerenes
95 ($C_{60}H_x$ or $C_{70}H_x$). The first study, by Loutfy, reported that
96 $C_{60}H_x$ performed similarly to pure C_{60} and that the electrode
97 dissolved during cycling showed minimal reversible capacity.²³
98 On the other hand, $C_{70}H_x$ showed some reversible
99 intercalation of lithium with a capacity of ~ 600 mAh/g;
100 however, only eight cycles were reported at a cycling rate with
101 a constant current rate of 0.1 C until a voltage of 0.005 V
102 followed by a constant voltage step (at 0.005 V) until 2% of
103 the constant current value is reached. Recently, the reversible
104 intercalation of sodium ions in $C_{60}H_x$ utilizing a poly(ethylene
105 oxide) (PEO)-based polymer electrolyte was demonstrated in
106 the solid state.²⁴ In this study, only one hydrogenated
107 fullerene, with an average of 39 hydrogen atoms chemically
108 attached to C_{60} , was evaluated. This material showed an initial
109 capacity of 230 mAh/g with a 10% capacity retention after 20
110 cycles when operated at 60 °C. Also, it has been demonstrated
111 that the presence of hydrogen on graphite significantly
112 enhanced the lithiation capacity of the material.²⁵ The
113 hydrogen atoms were transferred to the graphite via
114 mechanochemical milling with a rare earth hydride (YH_3).
115 The enhancement in the capacity demonstrated by the
116 graphite– YH_3 composite anode was attributed to the
117 formation of negatively charged sites on the graphite surface,
118 resulting in a higher number of lithium atoms that can be
119 stored per carbon atom ($Li_5C_{16}H$ versus LiC_6 for a graphite
120 electrode). The presence of hydrogen increased the capacity of
121 the hydrogen containing anode composite to 720 mAh/g.

122 In this current work, we wanted to completely rule out the
123 possible contribution of the yttrium metal (or its hydride) to
124 the anode capacity of a carbon-based anode and utilize a model
125 system in which the hydrogen content of the material can be
126 controlled. To achieve this, a series of hydrogenated fullerenes

($C_{60}H_x$) were prepared via heat and hydrogen overpressure 127
with pure C_{60} powder in one step.^{26,27} This approach would 128
allow one to fully examine the effect of hydrogen on the carbon 129
surface without any possible effects from a metal hydride (i.e., 130
 YH_3). To accomplish this, a systematic experimental and 131
theoretical study of lithium ion intercalation into a series of 132
hydrogenated fullerenes ($C_{60}H_x$) was performed. The average 133
number of hydrogen atoms (x) attached to C_{60} was varied 134
from 0 to 26 (0 to 3.44 wt %). Through this study we 135
determined that there is an optimal level of hydrogenation that 136
will facilitate reversible lithiation for 2000 cycles at high rates 137
of charge/discharge. This enhanced reversibility of lithium ion 138
intercalation in $C_{60}H_x$ is due to the electronic structure 139
changes, namely, the breaking of the surface C–C π -bonds, 140
which induces active/negatively charged carbon site, as 141
described through theoretical calculations. The $C_{60}H_{18}$ is 142
primarily studied as an example, which contains three active 143
carbon sites where Li cations would adsorb, resulting in the 144
observed voltage plateaus in the galvanostatic cycling study. 145
Based on the capacity of the material at a cycling rate of 0.05 146
A/g (~ 0.1 C), ~ 16 Li atoms can be stored per $C_{60}H_x$ 147
molecule, which is a significantly higher Li:C ratio than the 148
theoretical capacity of graphite currently utilized in commercial 149
lithium ion batteries (Li:6C for graphite versus Li:3.75C for 150
 $C_{60}H_x$). This unique approach to enhancing the capacity of 151
carbon-based anode materials can potentially lead to new high- 152
capacity anodes that can be tailored for other alkali and 153
alkaline earth metal batteries. 154

155 ■ EXPERIMENTAL SECTION

Materials. $LiPF_6$ in ethylene carbonate (EC):dimethyl carbonate 156
(DMC) was purchased from Novolyte. C_{60} and NMP were purchased 157
from Sigma-Aldrich. Acetylene black (AB) was purchased from Fisher. 158
Poly(vinylidene fluoride) (PVdF) was purchased from MTI Corp. 159

$C_{60}H_x$ Synthesis. The method for hydrogenating the C_{60} has been 160
previously described.²⁸ Briefly, the C_{60} was ground with a mortar and 161
pestle for 5 min to expose more surface area for hydrogenation inside 162
of an argon-filled glovebox. After grinding, the C_{60} turns from a shiny 163
black color to a dull brown color. In a typical hydrogenation reaction, 164
400 mg of ground C_{60} was loaded into a sample holder of a HyEnergy 165
PCT Pro 2000 (Sievert's Apparatus) and charged with 100 bar of H_2 . 166
A reservoir attached to the sample (175 mL) was also charged with 167
100 bar of H_2 . The sample was heated to 350 °C over the course 168
of 90 min and then soaked at that temperature for 6–72 h. 169
Immediately after completion of the hydrogenation, the sample was 170
cooled to room temperature and stored inside of the glovebox until 171
use. These sample conditions were utilized to minimize cage 172
fragmentation during the hydrogenation process as previously 173
reported.^{29–31} 174

Material Characterization. XRD was performed on a PAN- 175
alytical X'pert Pro with Cu $K\alpha$ radiation, and the samples were 176
protected with a Kapton film to minimize oxidation. SEM images 177
were acquired using a Hitachi SU8200 Series Ultimate Cold Field 178
Emission SEM with varying accelerating voltages and magnifications. 179
Samples were prepared in an Ar-filled glovebox and contained in Ar- 180
filled containers until transfer into the instrument. Air exposure during 181
sample insertion was < 5 s. Electrochemical testing was performed 182
using a Bio-Logic VMP3 multichannel potentiostat. 183

Cell Assembly and Testing. A dry powder anode composite 184
consisting of $C_{60}H_x$:acetylene black (AB):poly(vinylidene fluoride) 185
(PVdF) (8:1:1 weight ratio) was used in the initial screening tests. 186
For the screening tests ~ 1 – 2 mg of the anode composite was pressed 187
into a nickel foam current collector. No effect on the capacity was 188
observed for this loading amount. Swagelok type cells were then 189
assembled with the anode composite on Ni foam, glass fiber filter 190
paper as separator, Li metal as the counter/reference electrode, and 191

192 1.0 M LiPF₆ in EC:DMC as the liquid electrolyte. The cells were aged
193 for 12 h before any electrochemical tests were performed. For the
194 preparation of the C₆₀H_x (48 h) film on Cu foil current collector, the
195 same weight ratio of C₆₀H_x (48 h):AB:PVdF was used. The
196 components were homogenized via mortar and pestle for 5 min
197 before adding 1-methyl-2-pyrrolidinone (NMP) to make a thick
198 slurry. The slurry was then cast on Cu foil and heated to 80 °C over 1
199 h and soaked at that temperature for at least 18 h to yield a film with
200 good consistency and adhesion to the substrate. The typical loading of
201 active material was 1.1 mg on a 0.9 cm diameter Cu foil. This
202 translates to an active material loading of 1.7 mg/cm². The
203 galvanostatic cycling was performed at current densities from 0.05
204 to 1 A/g (~0.1 to 2 C) between 0.005 and 3.0 V vs Li. The
205 electrochemical impedance spectroscopy (EIS) measurements were
206 performed on the initial cell before cycling and after a certain number
207 of cycles for a test cell in a frequency range of 1 MHz–100 Hz. Cyclic
208 voltammetry was performed between 0.005 and 3.0 V vs Li at a rate of
209 0.05 mV/s.

210 **Computational Methods.** Our first-principles calculations are
211 based on spin-polarized density functional theory (DFT) with
212 generalized gradient approximation (GGA) for exchange-correlation
213 potential given by Perdew, Burke, and Ernzerhof (PBE),³² as
214 implemented in the Vienna Ab initio Simulation Package (VASP).³³
215 The projector augmented wave (PAW) method³⁴ was used to treat
216 the core electrons, while the valence electrons were represented by
217 using the plane wave basis set. The plane wave cutoff energy was set
218 to be 400 eV. The convergence criteria for energy and force were set
219 at 10⁻⁴ eV and 0.02 eV/Å, respectively.

220 ■ RESULTS AND DISCUSSION

221 To evaluate and understand the ability of C₆₀ to reversibly
222 intercalate Li⁺, five different quantities of hydrogen were
223 chemically attached to the molecule via heat (350 °C),
224 hydrogen pressure (100 bar of H₂), and time (6–72 h). The
225 addition of hydrogen to C₆₀ results in the expansion of the fcc
226 lattice parameter (*a*) in a linear fashion as previously
227 reported.³⁵ Based on the lattice expansion of the fcc lattice,
228 the average weight percent of hydrogen attached to the C₆₀ can
229 be determined. This analysis determined that there is 0.66,
230 0.94, 2.05, 2.5, and 3.44 wt % hydrogen attached for the 6, 12,
231 24, 48, and 72 h samples, respectively. This corresponds to an
232 average of 4, 8, 14, 18, and 26 hydrogen atoms per C₆₀
233 molecule for each of the samples, respectively. LDI-TOF-MS
234 was utilized to analyze the samples, which clearly showed the
235 hydrogenation of the C₆₀ was occurring (Figure S1).

236 The electrochemical properties of the hydrogenated full-
237erenes were determined by preparing a composite anode with
238 C₆₀H_x, acetylene black (AB), and poly(vinylidene fluoride)
239 (PVdF). The anode composites (1–2 mg) were then
240 compressed into a nickel foam disk. The nickel disk containing
241 the anode composite, a separator (glass fiber filter paper),
242 lithium metal, and 1.0 M LiPF₆ in EC:DMC (1:1 weight ratio)
243 were assembled in a Swagelok-type cell for cycling and cyclic
244 voltammetry studies. This allowed for the initial screening of
245 the samples to understand what quantity of hydrogen is
246 optimal for this type of application. The first galvanostatic
247 lithiation/delithiation cycle for each sample is shown in Figure
248 1a. All of the hydrogen-containing samples, except for the 72 h
249 sample, showed a higher capacity than pure C₆₀. Additionally,
250 all of the samples showed that lithiation of the hydrogenated
251 samples occurred at lower potentials than that of pure C₆₀. The
252 lithiation potentials are higher than that of graphite but lower
253 than lithium titanate (LTO). This is advantageous because it
254 would minimize/eliminate the formation of lithium dendrites
255 during lithiation of the anode and allow for a full cell to

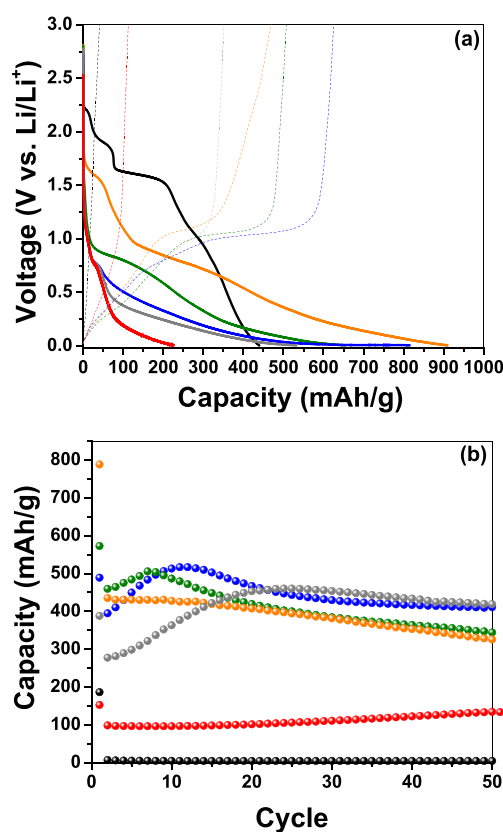


Figure 1. (a) First lithiation/delithiation cycle of the C₆₀H_x anodes at a current density of 0.025 mA/g. The lithiation is a solid line while the delithiation is a dashed line for C₆₀H_x with five different hydrogenation times (black: pure C₆₀; orange: 6 h = 0.66 wt %; green: 12 h = 0.94 wt %; blue: 24 h = 2.05 wt %; gray: 48 h = 2.5 wt %; red: 72 h = 3.44 wt %). (b) Capacity as a function of cycle number for C₆₀H_x with five different hydrogenation times. Cycling was performed at a current density of 0.05 A/g between 0.005 and 3.000 V vs lithium.

operate at a higher voltage than one using an LTO anode paired with a cathode.

The cycling data for the first 50 cycles of the C₆₀H_x samples at a 0.05 A/g current density are shown in Figure 1b. The pure C₆₀ sample showed an initial capacity of 186 mAh/g; however, the sample showed no capacity on subsequent cycles due to its solubility in the organic electrolyte, as expected. All of the other samples that contained hydrogen exhibited a sustainable reversible capacity over the first 50 cycles. For each of the hydrogenated samples, there is an initial rise in the capacity followed by a plateau after ~20 cycles. The hydrogen content also played a factor in the reversible capacity of the anode material with the 48 h hydrogenated sample (~2.5 wt %) showed the highest capacity retention after 50 cycles in this initial screening, and it was determined that this sample contained the optimal amount of chemically bound hydrogen for this type of application. This sample was selected for further characterization and will be the focus for the rest of the experimental and theoretical studies here after.

To obtain a consistent and uniform sample for further testing of the 48 h sample, a slurry of this material with NMP was prepared by using the same weight ratio of C₆₀H_x:AB:PVdF (8:1:1) and cast as a uniform film on a Cu foil current collector. The initial capacity of the slurry cast on Cu foil has a much lower capacity than what was observed for initial screening test where the dry powder was compressed

282 into Ni foam. We attribute this to the coating and shielding of
 283 the active material ($C_{60}H_x$) by the added conducting carbon
 284 and PVdF from the electrolyte solution during the slurry
 285 formation. The slurry allowed for an improved cycling
 286 performance over multiple cycles relative to the non-slurry
 287 samples shown in Figure 1. As Figure 2a shows, there is a

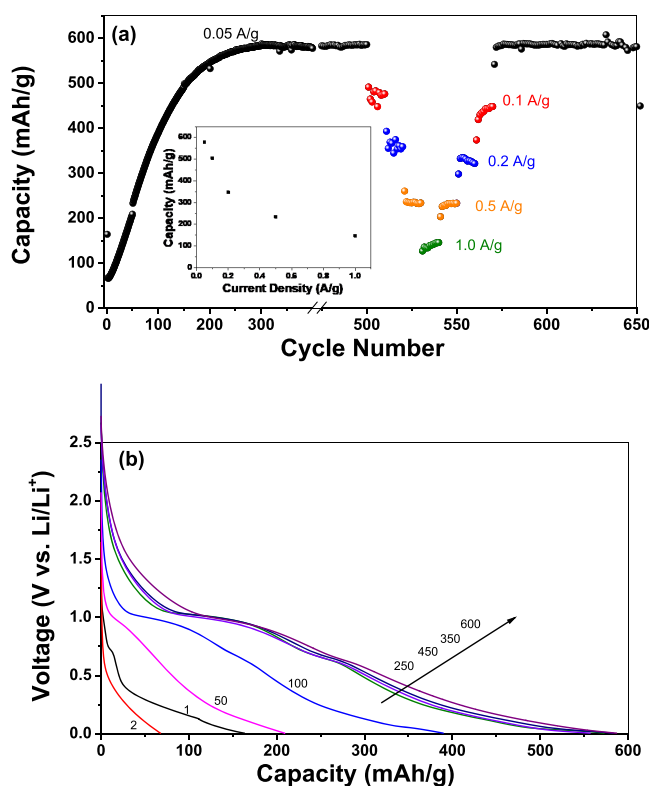


Figure 2. (a) Capacity vs cycle number for a $C_{60}H_x$ (48 h) anode on a Cu current collector. The current densities are listed for the cycles. Cycling was performed at a current density of 0.05, 0.1, 0.2, 0.5, and 1.0 A/g between 0.005 and 3.000 V vs lithium. Inset shows the average capacity as a function of current density. (b) Galvanostatic delithiation profile for selected cycles from the extended cycling study at 0.05 A/g.

288 gradual rise in the capacity as a function of cycle number over
 289 the first 300 cycles up to 588 mA/g, and this capacity holds
 290 steady for the next 300 cycles. After 500 cycles we examined
 291 the effect of different current densities (0.1, 0.2, 0.5, and 1.0 A/
 292 g, which correspond to 0.2, 0.4, 1, and 2 C, respectively). As
 293 expected, the capacity of the electrode decreases with an
 294 increase in current density due to internal resistance within the
 295 electrode. Upon returning to a 0.05 A/g cycling rate (0.1 C),
 296 the capacity returns to its steady state of ~ 580 mAh/g for the
 297 next 150 cycles, which indicates that this is a very stable and
 298 robust anode material. Figure 2b shows the voltage profiles for
 299 selected cycles during lithiation of the material. A gradual rise
 300 in the lithiation potential is observed with cycling which
 301 reaches a steady state after ~ 250 cycles. This steady-state
 302 lithiation profile corresponds to the plateau in the capacity of
 303 the anode (Figure 2a). Closer analysis of the voltage profile
 304 shows that there are three primary lithiation stages of the
 305 sample which occur at voltages of ~ 1.00 , 0.65, and 0.25 V.
 306 After ~ 25 cycles the plateau at ~ 1.00 V is the dominant
 307 lithiation event in this material and was observed in all of the
 308 $C_{60}H_x$ samples, except for the 72 h sample (Figures S2–S6).

This behavior was also consistent with the cyclic voltammetry
 experiments (Figures S7–S12).

The gradual rise in the capacity and change in voltage profile
 with cycling has been previously observed in other anode
 systems such as hierarchical porous carbons (HPC), porous
 carbon nanofiber webs, and nitrogen-doped carbon@graphene
 nanosheets.^{36–38} All of these high-capacity anodes demonstrate
 a significant increase in capacity as a function of cycling and is
 attributed to activation of the electrode. This increase in
 capacity is $>150\%$ of the original capacity for some of the
 materials with this activation process occurring over hundreds
 of lithiation/delithiation cycles. This same behavior observed
 during the cycling of $C_{60}H_x$ is attributed to the activation of
 the electrode via pulverization of the electrode, resulting in the
 exposure of more surface of the active material to the
 electrolyte resulting in the increased capacity up to the steady
 state. The lithiation of $C_{60}H_x$ also causes a slight increase in the
 crystalline lattice, which also opens more pathways for lithium
 diffusion and active sites for the lithium ion to attach to on the
 molecule. Once the electrode reaches a steady state (after
 ~ 250 cycles), a stable cycling capacity of the anode is
 observed. This is consistent with SEM and EIS (Figures S13–
 S18) analysis of the electrode during and after cycling. The
 pulverization and increase in porosity of the electrode before
 and after cycling are apparent in the SEM. In the precycled
 electrode on the Cu foil, the surface of the electrode is rough
 with high porosity while there is the formation of a compact
 layer deeper within the electrode with a very low porosity. This
 is attributed to the slurry casting method used and uniform
 distribution of the PVdF binder throughout the electrode when
 compared to the dry method utilized for the screening of the
 materials with the Ni foam current collector (Figure 1). This
 compact and low-porosity section below the surface of the
 electrode is inaccessible to lithium ion intercalation, resulting
 in the initial low capacity of the material. SEM imaging of the
 cycled electrode on Cu foil clearly shows the formation of a
 porous structure throughout the entire depth of the electrode.
 As the pulverization and activation process of the electrode
 takes place, the section once inaccessible to lithium ion
 intercalation is now accessible, resulting in the increase in
 capacity over the first 250 cycles (Figure 2).

The EIS data clearly show a reduction in the SEI surface
 layer resistance, the charge transfer resistance, and double-layer
 capacitance from the first cycle until the 800th cycle. This is
 attributed to the pulverization of the electrode with continued
 cycling with exposes more of the active surface to the
 electrolyte which results in the increasing capacity with cycle
 number. This is consistent with the SEM images with shows a
 reduction in particle size and increase in connectivity of the
 electrode with cycling. This is likely due to the expansion and
 contraction of the electrode upon lithiation/delithiation,
 respectively. Qualitative analysis of the EIS data derived from
 an equivalent circuit model of the system showed nearly a 2
 order increase in the Warburg impedance component from the
 initial state to the 1000th cycle. Because the Warburg
 impedance continually increases throughout cycling, this
 insinuates that the gravimetric capacity of the material should
 increase as well. We also observed a gradual decrease in the
 overall resistance of the cell with cycling up to the 800th cycle.
 This conductivity increase can be attributed to the activation of
 our material and in turn will lead to lower overpotentials and
 higher efficiencies in the cell, making it easier for effective
 lithium uptake. However, after 1000 cycles we start to see an

372 increase in electrochemical resistance; this insinuates the
373 potential decomposition of our material after prolonged
374 cycling which is reflected in the gradual decrease in capacity
375 after the 1000th cycle (Figure S19).

376 Ex situ XRD was also performed on the sample in the initial,
377 lithiated, and delithiated states (Figure S20). The XRD pattern
378 of initial state of the electrode ($C_{60}H_x$ -AB-PVdF) was
379 consistent with the pure $C_{60}H_x$ sample. After the first lithiation
380 of the electrode, the sharp diffraction peaks of the $C_{60}H_x$
381 become broader and less intense, indicating a relatively
382 amorphous product results. After the delithiation of the
383 electrode, the diffraction patterns associated with $C_{60}H_x$
384 reappear with some peak broadening, which indicate the
385 $C_{60}H_x$ is losing its crystallinity with increasing cycles. This
386 finding is also consistent with the activation process of the
387 electrode with cycling as determined by SEM, EIS, and
388 galvanostatic cycling. Next, we examined the cycle stability up
389 to 2000 cycles for rates of 0.1 and 0.5 A/g (0.2 and 1 C,
390 respectively) after 50 conditioning cycles at 0.05 A/g (0.1 C).
391 Even at high current density, the $C_{60}H_x$ (48 h) anode showed
392 good cycle stability and capacity over this extended cycling
393 study (Figure S19). When the cycling was switched to 0.1 A/g
394 there is a gradual rise in capacity up 550 mAh/g. This is
395 consistent with the steady-state capacity of a cell that was
396 cycled at 0.1 A/g. After the 2000 cycles, the capacity of the
397 anode still remains above 200 mAh/g at the high 0.5 A/g
398 current density.

399 The ability to reversibly store Li within the fullerene matrix
400 is not surprising based on prior work, which indicated that a
401 Li_4C_{60} system exhibits superionic conductivity.³⁹ Further NMR
402 of Li and Na intercalated C_{60} also supported the idea that alkali
403 metals can be mobile within the structure even in the presence
404 of high hydrogen content.^{40–42} This also includes clustering of
405 the lithium within the octahedral sites of the fcc lattice at
406 higher concentrations. The stable cycling in this system is
407 attributed to the reduced solubility of the C_{60} in the
408 hydrogenated state.

409 THEORETICAL SECTION

410 To complement experimental results, we studied the preferred
411 adsorption site of Li on $C_{60}H_x$ and its binding energy using
412 density functional theory and the VASP code as outlined in the
413 Experimental Section. Here, we used a single $C_{60}H_x$ molecule
414 to study the adsorption of Li atoms. Note that the interaction
415 between adjacent molecules in the $C_{60}H_x$ molecular crystal is
416 usually weak; thus, the properties of the bulk can be
417 understood by focusing on an isolated molecule. A vacuum
418 space of 25 Å along the x , y , and z directions was adopted to
419 avoid interactions between neighboring images. To understand
420 the underlying mechanism responsible for the enhanced
421 lithiation capacity of $C_{60}H_x$, we first studied the adsorption
422 behavior of a single Li atom on $C_{60}H$ and $C_{60}H_2$. In $C_{60}H$ the
423 charge on the H atom was found to be positive while the C
424 atom next to the adsorption site is charged negatively (Figure
425 3a,b). This is similar to the situation found on hydrogenated
426 graphite. When lithiated, the Li atom prefers to bind to the
427 negatively charged center. The binding energies of Li in $C_{60}Li$
428 and $C_{60}HLi$ are respectively 1.58 and 2.02 eV. Thus, the Li
429 atom is bound more strongly to $C_{60}H$ compared to pure C_{60} ,
430 again consistent with the results found on hydrogenated
431 graphite. This mechanism can be understood by knowing that
432 hydrogenation breaks the π bonds between $C-p_z$ orbitals and
433 creates active carbon sites on the surface, which then enhances

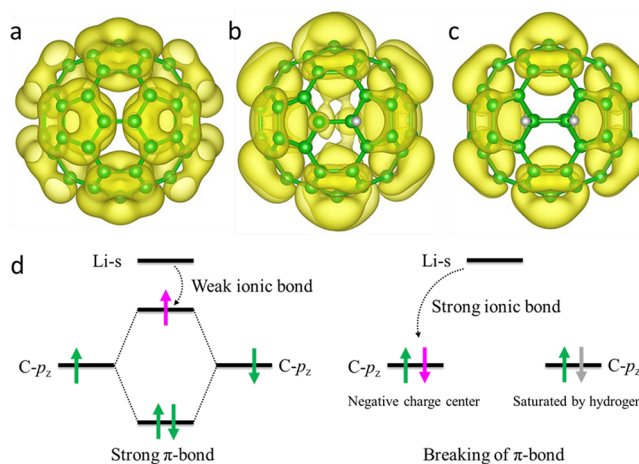


Figure 3. Hole density isosurface of LUMO for pure (a) C_{60} , (b) $C_{60}H$, and (c) $C_{60}H_2$. (d) Schematic diagram for enhancement of Li adsorption by hydrogenation.

the ionic bond between Li-s and $C-p_z$ orbitals (see Figure 3d).⁴³⁴
The binding characteristics of Li changes as the hydrogen
435 content of $C_{60}H_x$ increases. For example, the binding energy of
436 Li in $C_{60}H_2Li$ is 1.57 eV, which is nearly the same as that in
437 $C_{60}Li$ (1.58 eV). This is because the Li atom prefers to adsorb
438 on a pentagon-center-top site far away from the adsorbed
439 hydrogen site as no negatively charged center is observed in
440 $C_{60}H_2$ (Figure 3c). These results indicate that a negatively
441 charged center, induced by hydrogenation, is crucial for
442 stronger binding of Li on $C_{60}H_x$.⁴⁴³

Next, we focused on the Li adsorption on $C_{60}H_{18}$ and
444 compared that to results on pure C_{60} . This is because $C_{60}H_{18}$
445 (~ 2.5 wt % H) was optimal for lithiation capacity according to
446 our experimental results, and the geometry of $C_{60}H_{18}$ has been
447 previously well-established. We took the initial geometries of
448 C_{60} and $C_{60}H_{18}$ from the literature and fully relaxed them. We
449 present the computed geometry of $C_{60}H_{18}$ in Figure 4. To
450 determine the optimal configurations of $C_{60}Li_n$ and $C_{60}H_{18}Li_n$
451 is a difficult task as there are numerous possible adsorption
452 sites of Li atoms. On the basis of our previous results on
453 $C_{60}HLi_n$ and $C_{60}H_2Li_n$, we chose the initial configurations of
454 $C_{60}H_{18}Li_n$ by following the following guidelines: (i) The
455 geometry of the n th candidate is based on the optimal
456 configuration of $C_{60}H_{18}Li_{n-1}$. (ii) Li atoms should adsorb close
457 to the active sites (if it exists) on the molecular surface. (iii) Li
458 atoms should reside away from H atoms because of
459 electrostatic repulsion. (iv) The usual possible adsorption
460 sites of Li atoms on $C_{60}H_x$ are on top of the pentagon center,
461 the hexagon center, C–C bridge, and C-sites. For each value of
462 n we have considered at least 10 possible adsorption sites for
463 Li.⁴⁶⁴

Our calculations show that Li atoms prefer to adsorb on top
465 of the pentagon center on pure C_{60} and distribute uniformly on
466 its surface. This is consistent with previous studies.^{43,44} The
467 binding energy of each Li atom [defined as $E_b(n) =$
468 $E(C_{60}Li_{n-1}) + E(\text{isolated Li atom}) - E(C_{60}Li_n)$] gradually
469 decreases with the number of Li atoms up to $n = 18$. Three
470 stages are observed in the binding energy profile, namely, the
471 average binding energies of the first six, second six, and third
472 six are 1.73, 1.37, and 0.99 eV, respectively. Interestingly, these
473 three stages of binding energy can also be deduced from the
474 electronic energy levels of conduction states near the Fermi
475 level, where, for instance, the 3-fold LUMO state corresponds
476

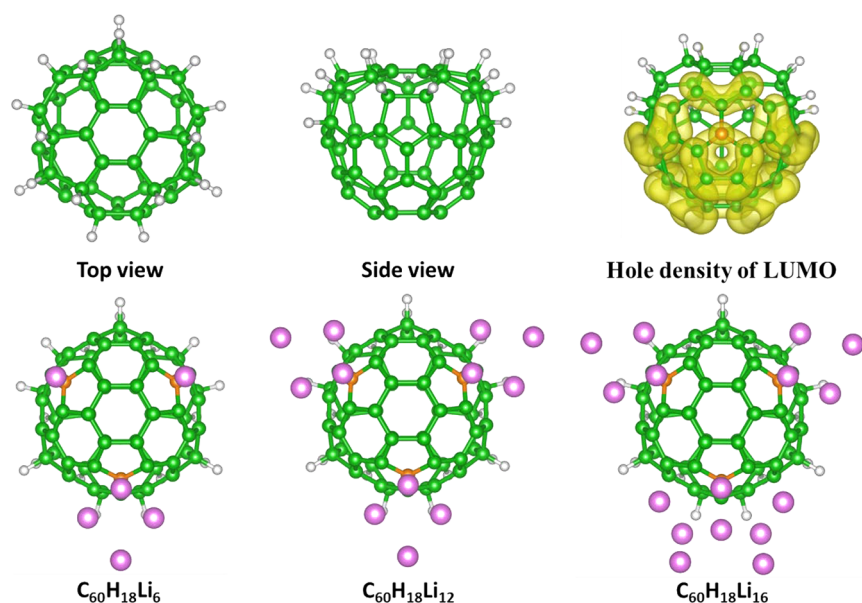


Figure 4. Top and side views of atomic structure for C₆₀H₁₈, hole density isosurface of LUMO for C₆₀H₁₈, and optimal structures for C₆₀H₁₈Li₆, C₆₀H₁₈Li₁₂, and C₆₀H₁₈Li₁₆. Green, gray, and pink balls represent C, H, and Li atoms, respectively. Orange balls represent active C-sites.

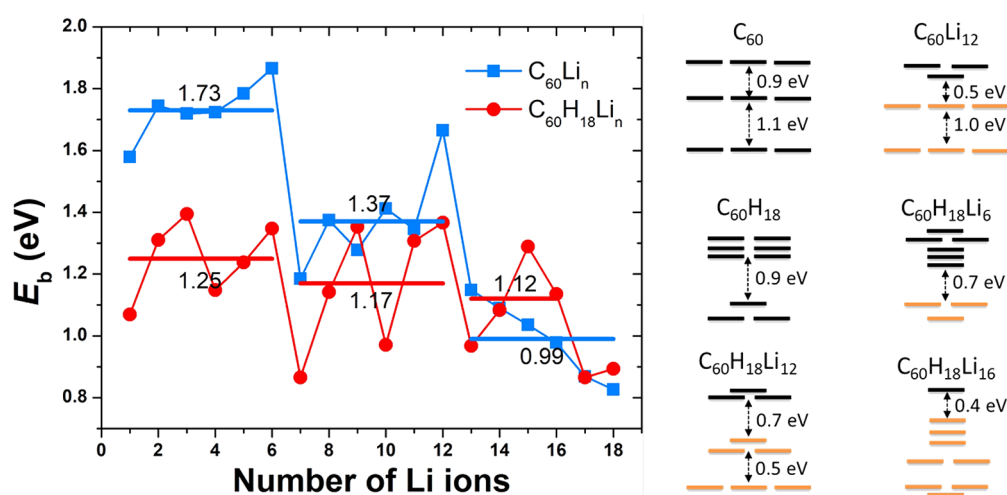


Figure 5. Binding energy of each Li ion on C₆₀ and C₆₀H₁₈ as a function of number of Li ions (left). Energy levels near the Fermi energy for C₆₀, C₆₀Li₁₂, C₆₀H₁₈, C₆₀H₁₈Li₆, C₆₀H₁₈Li₁₂, and C₆₀H₁₈Li₁₆ (right). Orange and black lines represent occupied and unoccupied states, respectively.

477 to the first stage because each Li atom adds one valence
478 electron, and the adsorption of six Li atoms fulfills the LUMO
479 state. The large gap between electronic energy levels is the
480 reason for sharp increase in E_b . It is known that original C₆₀ has
481 a lithiation capacity of ~ 12 Li per C₆₀, suggesting that the third
482 stage with a binding energy of 0.99 eV is a cutoff for Li
483 adsorption.

484 Next, we explore the case of C₆₀H₁₈, where very different
485 behavior of Li adsorption is observed. We found that the Li
486 atoms favor to adsorb around three specific C-sites instead of
487 uniformly distributing over C₆₀ (Figure 4). This is because
488 hydrogenation breaks the π -bonds and induces active sites/
489 negative charge centers on the surface, which bind strongly to
490 Li atoms. This can be confirmed by the hole density of LUMO,
491 which shows three isolated C-sites (marked by orange)
492 localized charges, similar to the C₆₀H case. Consequently, Li
493 atoms are expected to bind more strongly with C₆₀H₁₈ than
494 C₆₀. We calculated the binding energy of each Li atom on
495 C₆₀H₁₈ using the formula $E_b(n) = E(\text{C}_{60}\text{H}_{18}\text{Li}_{n-1}) + E(\text{isolated}$

Li atom) $- E(\text{C}_{60}\text{H}_{18}\text{Li}_n)$. The binding energy profiles of Li
496 atoms on C₆₀ and C₆₀H₁₈ have different trend. For $n < 13$, the
497 binding energy of Li on pure C₆₀ is larger than that on C₆₀H₁₈.
498 Reverse is the case when $n > 13$. For example, the calculated
499 binding energy of the first Li atom on C₆₀H₁₈, namely 1.07 eV,
500 is smaller than that on C₆₀ (1.58 eV). This can be explained by
501 the fact that the HOMO–LUMO gap of C₆₀H₁₈ (2.29 eV) is
502 larger than that of C₆₀ (1.64 eV). From the electronic energy
503 levels of conduction states around the Fermi energy, we also
504 find three stages separated by large energy gaps (>0.4 eV) for
505 n ranging from 1 to 16 (Figure 5). These are $n = 1-6$ (1.25 eV),
506 $n = 7-12$ (1.17 eV), and $n = 13-16$ (1.12 eV), corresponding
507 to the three voltage plateaus (~ 1.00 , 0.65, and 0.25 V),
508 observed experimentally. The average binding energies of first
509 and second stages are smaller than those of C₆₀, while that of
510 the third stage (1.12 eV) is larger than that of C₆₀ (0.99 eV),
511 suggesting that C₆₀H₁₈ can adsorb more Li atoms than C₆₀.
512 When $n > 16$, E_b becomes small (<0.9 eV). These results
513

514 explain the improved lithiation capacity (~ 16 Li per $C_{60}H_{18}$)
515 of $C_{60}H_{18}$ compared with pure C_{60} .

516 On the basis of the above analysis, we conclude that the key
517 to enhancing the lithiation capacity of $C_{60}H_x$ is breaking of the
518 C–C π -bonds, which induces active sites/negative charge
519 centers on the surface. When x is small, the electrostatic
520 repulsion between hydrogen atoms is small, and an even
521 number of hydrogen atoms can adsorb on the neighboring C-
522 sites, forming strong covalent bonds and stabilizing the surface.
523 At intermediate hydrogen content, e.g., $x = 18$, the electrostatic
524 repulsion between hydrogen atoms becomes strong enough to
525 separate the adsorption sites of hydrogen atoms. In this case,
526 the C–C π -bonds are broken by hydrogenation and active/
527 negatively charged C-sites appear on the surface. When x
528 becomes even larger, the surface of C_{60} is mostly covered with
529 hydrogen atoms, and the repulsion between hydrogen atoms
530 and Li atoms becomes rather strong. This makes the
531 adsorption of Li atoms more difficult. For instance, the
532 binding energy of the first Li atom on $C_{60}H_{26}$ is as small as 0.78
533 eV. This finding is consistent with the low capacity observed
534 experimentally for the highly hydrogenated 72 h sample, which
535 has an average hydrogen content of $C_{60}H_{24}$ and a capacity of
536 only 135 mAh/g after 50 cycles. Therefore, a moderate value
537 of x is preferable for improving the lithiation capacity of $C_{60}H_x$.

538 ■ CONCLUSION

539 We have demonstrated that the addition of chemically bound
540 hydrogen can be used to manipulate the physical and
541 electronic properties of C_{60} , allowing it to be used as a high-
542 capacity anode for reversible lithium ion intercalation. It was
543 determined that a sample containing ~ 2.5 wt % H ($\sim C_{60}H_{18}$)
544 was optimal for this application. The chemisorbed hydrogen
545 creates three negatively charged active sites on the C_{60} for
546 lithium to adsorb and cause an expansion and pulverization of
547 the electrode material. This process allows for the flow of
548 lithium ions during galvanostatic cycling. By fine-tuning the
549 amount of chemisorbed hydrogen on the anode material, we
550 can effectively optimize this and similar materials to serve as
551 ubiquitous hosts of various alkali and alkaline earth metals. We
552 are currently investigating the ability of this class of materials
553 for the intercalation of other monovalent (Na^+ , K^+) and
554 divalent (Mg^{2+}) cations and will be reported in due course.

555 ■ ASSOCIATED CONTENT

556 ■ Supporting Information

557 The Supporting Information is available free of charge on the
558 ACS Publications website at DOI: 10.1021/acs.aem.9b01040.

559 Additional experimental characterization: XRD, LDI-
560 TOF-MS, galvanostatic charge/discharge, CV, EIS, and
561 SEM (PDF)

562 ■ AUTHOR INFORMATION

563 Corresponding Authors

564 *(J.A.T.) E-mail: joseph.teprovich@csun.edu.

565 *(P.J.) E-mail: pjena@vcu.edu.

566 ORCID

567 Joseph A. Teprovič, Jr.: 0000-0002-7285-4844

568 Chengxi Huang: 0000-0003-1491-3954

569 Jian Zhou: 0000-0002-2606-4833

570 Puru Jena: 0000-0002-2316-859X

Author Contributions

J.A.T., R.Z., and P.J. conceived, guided, and directed the
experimental and computational work. J.A.W., P.A.W., and
S.C.T. performed the experimental characterization. C.H. and
J.Z. performed the theoretical calculations. The manuscript was
written with input and contributions by all authors.

Funding

This work was supported by the U.S. Department of Energy,
Office of Science, Basic Energy Sciences, Materials Sciences
and Engineering Division, and the Savannah River National
Laboratory LDRD program.

Notes

The authors declare no competing financial interest.

■ REFERENCES

- (1) Hebard, A. F.; Rosseinsky, M. J.; Haddon, R. C.; Murphy, D. W.;
Glarum, S. H.; Palstra, T. T. M.; Ramirez, A. P.; Kortan, A. R.
Superconductivity at 18K in potassium-doped C_{60} . *Nature* **1991**, *350*,
600–601.
- (2) Kelty, S. P.; Chen, C.; Lieber, C. M. Superconductivity at 30K in
caesium-doped C_{60} . *Nature* **1991**, *352*, 223–225.
- (3) Rosseinsky, M. J.; Ramirez, A. P.; Glarum, S. H.; Murphy, D. W.;
Haddon, R. C.; Hebard, A. F.; Palstra, T. T. M.; Kortan, A. R.;
Zahurak, S. M.; Makhija, A. V. Superconductivity at 28K in Rb_xC_{60} .
Phys. Rev. Lett. **1991**, *66*, 2830.
- (4) Zhang, R.; Mizuno, F.; Ling, C. Fullerenes: non-transition metal
clusters as rechargeable magnesium battery cathodes. *Chem. Commun.*
2015, *51*, 1108–1111.
- (5) Najafi, M. Application of C_{60} , C_{72} and carbon nano tubes as
anode for lithium-ion batteries: A DFT study. *Mater. Chem. Phys.*
2017, *195*, 195–198.
- (6) Matsushita, T.; Ishii, Y.; Kawasaki, S. Sodium ion battery
properties anode properties of empty and C_{60} -inserted single walled
carbon nanotubes. *Mater. Express* **2013**, *3*, 30–36.
- (7) Wang, F. F.; Wang, C.; Liu, R. Q.; Tian, D.; Li, N. Experimental
study on the preparation of Ag nanoparticle doped fullerene for
lithium ion battery application. *J. Phys. Chem. C* **2012**, *116*, 10461–
10467.
- (8) Zhou, F.; Jehoulet, C.; Bard, A. J. Reduction and electro-
chemistry of C_{60} in liquid ammonia. *J. Am. Chem. Soc.* **1992**, *114*,
11004–11006.
- (9) Jehoulet, C.; Obeng, Y. S.; Kim, Y.; Zhou, F.; Bard, A. J.
Electrochemistry and Langmuir trough studies of C_{60} and C_{70} films. *J.*
Am. Chem. Soc. **1992**, *114*, 4237–4247.
- (10) Matsuo, Y.; Nakajima, T. Electrochemical properties of
fluorinated fullerene C_{60} . *Electrochim. Acta* **1996**, *41*, 15–19.
- (11) Seger, L.; Wen, L.-Q.; Schlenhoff, J. B. Prospect for using C_{60}
and C_{70} in lithium batteries. *J. Electrochem. Soc.* **1991**, *138*, L81–L82.
- (12) Chabre, Y.; Djurado, D.; Armand, M.; Romanow, W. R.;
Coustel, N.; McCauley, J. P.; Fischer, J. E.; Smith, A. B.
Electrochemical intercalation of lithium into solid C_{60} . *J. Am. Chem.*
Soc. **1992**, *114*, 764–766.
- (13) Dalchiele, E. A.; Rosolen, J. M.; Decker, F. Electrochemically
intercalated M_xC_{60} thin films in a solid state cell ($M = Li, K$); optical
and photoelectrochemical characterization. *Appl. Phys. A: Mater. Sci.*
Process. **1996**, *63*, 487–494.
- (14) Lemont, S.; Ghanbaja, J.; Billaud, D. Electrochemical
intercalation of sodium ions into fullerene. *Mater. Res. Bull.* **1994**,
29, 465–472.
- (15) Huang, Z.; Chen, Y.; Cai, R.; Rui, C.; Zhang, F. First
electrochemical intercalation of lithium into fullerenated poly(*N*-
vinylcarbazole). *J. Appl. Polym. Sci.* **1996**, *60*, 573–577.
- (16) Kawabe, S.-i.; Kawai, T.; Sugimoto, R.-i.; Yagasaki, E.; Yoshino,
K. Electrochemical properties of fullerene derivative polymers as
electrode materials. *Jpn. J. Appl. Phys.* **1997**, *36*, L1055–L1058.

- (17) Liu, N.; Touhara, H.; Okino, F.; Kawasaki, S.; Nakacho, Y. Solid-state lithium cells based on fluorinated fullerene cathodes. *J. Electrochem. Soc.* **1996**, *143*, 2267–2272.
- (18) Shan, C.; Yen, H.; Wu, K.; Lin, Q.; Zhou, M.; Guo, X.; Wu, D.; Zhang, H.; Wu, G.; Wang, H. Functionalized fullerenes for highly efficient lithium ion storage: Structure property-performance correlation with energy implications. *Nano Energy* **2017**, *40*, 327–335.
- (19) Teprovich, J. A., Jr.; Wellons, M. S.; Lascola, R.; Hwang, S.; Ward, P.; Compton, R. N.; Zidan, R. Synthesis and Characterization of a Lithium Doped Fullerene ($\text{Li}_x\text{C}_{60}\text{H}_y$) for Reversible Hydrogen Storage. *Nano Lett.* **2012**, *12*, 582–589.
- (20) Knight, D. A.; Teprovich, J. A., Jr.; Peters, B.; Summers, A.; Ward, P. A.; Compton, R. N.; Zidan, R. Synthesis, Characterization, and Reversible Hydrogen Sorption Study of a Sodium-doped Fullerene. *Nanotechnology* **2013**, *24*, 455601.
- (21) Mauron, P.; Remhof, A.; Bliersbach, A.; Borgschulte, A.; Zuttel, A.; Sheptyakov, D.; Gaboardi, M.; Choucair, M.; Pontiroli, D.; Aramini, M.; Gorreri, A.; Riccò, M. Reversible hydrogen absorption in sodium intercalated fullerenes. *Int. J. Hydrogen Energy* **2012**, *37*, 14307–14314.
- (22) Ward, P. A.; Teprovich, J. A.; Compton, R. N.; Schwartz, V.; Veith, G. M.; Zidan, R. Evaluation of the Physico- and Chemisorption of Hydrogen in Alkali (Na, Li) Doped Fullerenes. *Int. J. Hydrogen Energy* **2015**, *40*, 2710–2716.
- (23) Loutfy, R. O.; Katagiri, S. Fullerene materials for lithium-ion battery applications. In *Perspectives of Fullerene Nanotechnology*; Springer: Dordrecht, Netherlands, 2002; pp 357–367.
- (24) Scaravonati, S.; Magnani, G.; Gaboardi, M.; Allodi, G.; Riccò, M.; Pontiroli, D. Electrochemical intercalation of fullerene and hydrofullerene with sodium. *Carbon* **2018**, *130*, 11–18.
- (25) Zheng, X.; Yang, C.; Chang, X.; Wang, T.; Ye, M.; Lu, J.; Zhou, H.; Zheng, J.; Li, X. Synergism of Rare Earth Trihydrides and Graphite in Lithium Storage: Evidence of Hydrogen-Enhanced Lithiation. *Adv. Mater.* **2018**, *30*, 1704353.
- (26) Luzan, S. M.; Tsybin, Y. O.; Talyzin, A. V. Reaction of C_{60} with Hydrogen Gas: In Situ Monitoring and Pathways. *J. Phys. Chem. C* **2011**, *115*, 11484–11492.
- (27) Talyzin, A. V.; Tsybin, Y. O.; Schaub, T. M.; Mauron, P.; Shulga, Y. M.; Zuttel, A.; Sundqvist, B.; Marshall, A. G. Composition of Hydrofullerene Mixtures Produced by C_{60} Reaction with Hydrogen Gas Revealed by High-Resolution Mass Spectrometry. *J. Phys. Chem. B* **2005**, *109*, 12742–12747.
- (28) Teprovich, J. A.; Washington, A. L.; Dixon, J.; Ward, P. A.; Christian, J. H.; Peters, B.; Zhou, J.; Giri, S.; Sharp, D. N.; Velten, J. A.; Compton, R. N.; Jena, P.; Zidan, R. Investigation of Hydrogen Induced Fluorescence in C_{60} and its Potential use in Luminescent Down Shifting Applications. *Nanoscale* **2016**, *8*, 18760–18770.
- (29) Talyzin, A.; Sundqvist, B.; Shulga, Y. M.; Peera, A. A.; Imus, P.; Billups, W. E. Gentle fragmentation of C_{60} by strong hydrogenation: a route to synthesizing new materials. *Chem. Phys. Lett.* **2004**, *400*, 112–116.
- (30) Talyzin, A. V.; Luzan, S.; Anoshkin, I. V.; Nasibulin, A. G.; Kauppinnen, E. I.; Dzwilewski, A.; Kreta, A.; Jamnik, J.; Hassanien, A.; Lundstedt, A.; Grennberg, H. Hydrogen-Driven Cage Unzipping of C_{60} into Nano-Graphenes. *J. Phys. Chem. C* **2014**, *118*, 6504–6513.
- (31) Talyzin, A. V.; Tsybin, Y. O.; Purcell, J. M.; Schaub, T. M.; Shulga, Y. M.; Noreus, D.; Sato, T.; Dzwilewski, A.; Sundqvist, B.; Marshall, A. G. Reaction of Hydrogen Gas with C_{60} at Elevated Pressure and Temperature: Hydrogenation and Cage Fragmentation. *J. Phys. Chem. A* **2006**, *110*, 8528–8534.
- (32) Perdew, J. P.; Burke, K.; Ernzerhof, M. Generalized Gradient Approximation Made Simple. *Phys. Rev. Lett.* **1996**, *77*, 3865–3868.
- (33) Kresse, G.; Hafner, J. Ab-initio molecular dynamics for liquid metals. *Phys. Rev. B: Condens. Matter Mater. Phys.* **1993**, *47*, 558–561.
- (34) Blochl, P. E. Projector augmented-wave method. *Phys. Rev. B: Condens. Matter Mater. Phys.* **1994**, *50*, 17953–17979.
- (35) Talyzin, A. V.; Shulga, Y. M.; Jacob, A. Comparative study of hydrofullerides C_{60}H_x prepared by direct and catalytic hydrogenation. *Appl. Phys. A: Mater. Sci. Process.* **2004**, *78*, 1005–1010.
- (36) Zhao, J.; Wen, X.; Xu, H.; Wen, Y.; Lu, H.; Meng, X. Salting-out and salting-in of protein: A novel approach toward fabrication of hierarchical porous carbon for energy storage application. *J. Alloys Compd.* **2019**, *788*, 397–406.
- (37) Qie, L.; Chen, M.; Wang, Z.; Shao, Q.; Li, X.; Yuan, L.; Hu, X.; Zhang, W.; Huang, Y. Nitrogen-Doped Porous Carbon Nanofiber Webs as Anodes for Lithium Ion Batteries with a Superhigh Capacity and Rate Capability. *Adv. Mater.* **2012**, *24*, 2047–2050.
- (38) Gayathri, S.; Arunkumar, P.; Kim, E.; Kim, S.; Kang, I.; Han, J. Mesoporous nitrogen-doped carbon@graphene nanosheets as ultra-stable anode for lithium-ion batteries - Melamine as surface modifier than nitrogen source. *Electrochim. Acta* **2019**, *318*, 290–301.
- (39) Riccò, M.; Belli, M.; Mazzani, M.; Pontiroli, D.; Quintavalle, D.; Jánosy, A.; Csányi, G. Superionic conductivity in the Li_4C_{60} fulleride polymer. *Phys. Rev. Lett.* **2009**, *102*, 145901.
- (40) Maidich, L.; Pontiroli, D.; Gaboardi, M.; Lenti, S.; Magnani, G.; Riva, G.; Carretta, P.; Milanese, C.; Marini, A.; Ricco, M.; Sanna, S. Investigation of Li and H dynamics in Li_6C_{60} and $\text{Li}_6\text{C}_{60}\text{H}_y$. *Carbon* **2016**, *96*, 276–284.
- (41) Sarzi Amadé, N.; Gaboardi, M.; Magnani, G.; Riccò, M.; Pontiroli, D.; Milanese, C.; Girella, A.; Carretta, P.; Sanna, S. H and Li dynamics in $\text{Li}_{12}\text{C}_{60}$ and $\text{Li}_{12}\text{C}_{60}\text{H}_y$. *Int. J. Hydrogen Energy* **2017**, *42*, 22544–22550.
- (42) Sarzi Amadé, N.; Pontiroli, D.; Maidich, L.; Riccò, M.; Gaboardi, M.; Magnani, G.; Carretta, P.; Sanna, S. Molecular and ionic dynamics in $\text{Na}_x\text{Li}_{6-x}\text{C}_{60}$. *J. Phys. Chem. C* **2017**, *121*, 6554–6560.
- (43) Sun, Q.; Jena, P.; Wang, Q.; Marquez, M. First Principles Study of Hydrogen Storage on $\text{Li}_{12}\text{C}_{60}$. *J. Am. Chem. Soc.* **2006**, *128*, 9741–9745.
- (44) Zimmermann, U.; Malinowski, N.; Burkhardt, A.; Martin, T.P. Metal-coated fullerenes. *Carbon* **1995**, *33*, 995–1006.